Traversability Estimation for a Planetary Rover via Experimental Kernel Learning in a Gaussian Process Framework

Ken Ho, Thierry Peynot and Salah Sukkarieh

***Abstract*— A critical requirement for safe autonomous navigation of a planetary rover is the ability to accurately estimate the traversability of the terrain. This work considers the problem of predicting the attitude and configuration angles of the platform from terrain representations that are often incomplete due to occlusions and sensor limitations. Using Gaussian Processes (GP) and exteroceptive data as training input, we can provide a continuous and complete representation of terrain traversability, with uncertainty in the output estimates. In this paper, we propose a novel method that focuses on exploiting the explicit correlation in vehicle attitude and configuration during operation by learning a kernel function from vehicle experience to perform GP regression. We provide an extensive experimental validation of the proposed method on a planetary rover. We show significant improvement in the accuracy of our estimation compared with results obtained using standard kernels (Squared Exponential and Neural Network), and compared to traversability estimation made over terrain models built using state-of-the-art GP techniques.**

I. Introduction

A critical requirement for safe autonomous navigation of a planetary rover is the ability to accurately estimate terrain *traversability* [1]. Traversability can be represented by aspects such as roughness of the terrain [2], [3], expected energy required to traverse it, or risk for the platform to tip over or slip [4]. Arguably, traversability metrics should be platform-dependent, since the difficulty of traversing terrain depends on the scale and capabilities of the platform (e.g. wheel size, weight distribution, chassis configuration, existence and type of suspension).

The fundamental aspect of traversability considered in this paper is represented by the attitude of the platform (pitch, roll) and the configuration of the chassis, which are respectively associated with the vehicle stability and the difficulty that the vehicle experiences in traversing over the terrain. State-of-the-art techniques to predict the rover's attitude and configuration angles on rough terrain using kinematic modeling on a digital elevation map (DEM) have been proposed (e.g. [5], [6]). However, they assume perfect and complete knowledge of the geometry of the underlying terrain, and use a deterministic model of the rover's kinematics. In practice, uncertainties in the terrain model (due to sensor errors, discretization etc.) and in the vehicle response can be significant and need to be considered.

The work was supported by the Australian Research Council, Australian Space Research Program Stream A, Pathways to Space: Empowering the Internet Generation, and the Australian Centre for Field Robotics (ACFR). This material is also based on research partially sponsored by the Air Force Research Laboratory, under agreement number FA2386-10-1-4153. The U.S. Government is authorized to reproduce and distribute reprints for Governmental purposes notwithstanding any copyright notation thereon.

K. Ho, T. Peynot and S. Sukkarieh are with the Australian Centre for Field Robotics, University of Sydney, NSW 2006, Australia, (k.ho,tpeynot,salah)@acfr.usyd.edu.au.

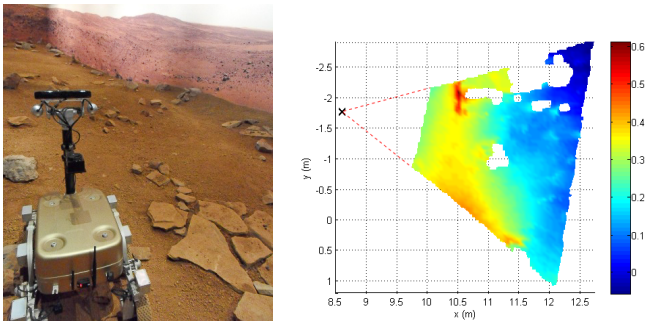

(a) (b)

Fig. 1. (a) Mawson rover in the Marsyard. (b) DEM of the terrain seen by the rover (indicated by the cross on the left), colored by elevation. Occluded areas are in white.

Slip prediction has been extensively studied in the literature of planetary rover exploration [4], [7]. Recently, various approaches have been introduced to classify visible terrain and predict slip from a database of terrain parameters [8], or learn parameters to estimate vehicle behavior via terramechanics models [7]. However, these approaches rely on expert knowledge of the traversability cost of each terrain type and they require accurate and complete models of the terrain geometry and of the configuration and attitude of the rover. Therefore, the ability to predict these attitude and configuration angles at any location on the terrain surrounding the rover is crucial for these methods as well.

Terrain representations built from onboard sensor data are often incomplete due to occlusions (illustrated by the "shadows" behind rocks in Fig. 1) and limitations in the sensor's field of view or resolution. Therefore, the resulting traversability map is often incomplete. To ensure the safety of an outdoor ground robot, the commonly accepted recommendation has been to consider non-observed areas as non traversable [9]. However, relatively small gaps in the terrain data can be frequent enough such that the rover cannot afford to avoid them all. Therefore, in practice, existing rover navigation algorithms usually avoid large gaps (which may not always be necessary) but ignore those that are small [5] (which might be dangerous). Instead, the method proposed in this paper can provide an accurate estimate of traversability in these occluded areas with associated uncertainty.

In this paper, we propose to predict the rover's attitude and configuration angles by learning the vehicle response on unstructured terrain from experience. The approach focuses

on exploiting the explicit correlation in vehicle attitude and configuration during operation. We propose an architecture for estimating the kernel function based on vehicle experience in a manner that would better represent the evolution of vehicle states and propagation of uncertainty. Gaussian Process (GP) regression, using exteroceptive data as training input, then provides a continuous representation of vehicle attitude and configuration over the terrain, with uncertainty in the output estimates and accurate estimation of traversability in areas with little or no exteroceptive data. We provide an extensive experimental validation of the proposed method on our planetary rover prototype. We show the improvement in the performance of our estimation via kernel learning compared with results obtained using standard kernels (Squared Exponential and Neural Network). We also show the improvement obtained compared to the prediction of the angles made using kinematic modeling on terrain models built via state-of-the-art GP techniques.

The paper is organized as follows. Sec. II discusses related work on terrain modeling and traversability estimation using GPs. Sec. III describes the proposed approach to estimate traversability via learning in the space of vehicle states. We describe the implementation of the approach on our experimental rover including experiment setup for validation in Sec. IV. In Sec. V we examine the results from our experiments and the impact of the approach on traversability estimation. Finally, Sec. VI proposes a conclusion and elements of future work.

II. Terrain Modelling and Traversability Estimation using GP

Kinematic modeling methods have been used to estimate terrain traversability based on vehicle structure and terrain geometry (DEM) [5], see DEM-Kin. in Fig. 2. However, DEMs built from inboard sensor data are often incomplete due to occlusions and sensor's limitations. As a result, DEM-Kin provides incomplete traversable maPS.

Regression methods have been used to determine a continuous terrain representation from incomplete terrain data. Gaussian Process (GP) regression is a popular method because of its versatility in dealing with uncertainty. Recent literature has proposed techniques to use GP regression to estimate Terrain Geometry (GP-TG) in areas with little or no data [10], [11] to produce a complete Continuous Elevation Map (CEM). However, the link with traversable estimation largely remains to be established.

In previous work [12], the authors have shown that predicting the vehicle response on such continuous terrain models, estimated via GP regression, using kinematics modeling could then lead to complete continuous traversability maps. This approach, referred to as GP-TG-Kin in Fig. 2 and the remainder of this paper, partially addresses the problems created by incomplete maps. However, the terrain models that have been estimated through this process have often been smoothed, thereby making the terrain appear to be easier to traverse than in reality.

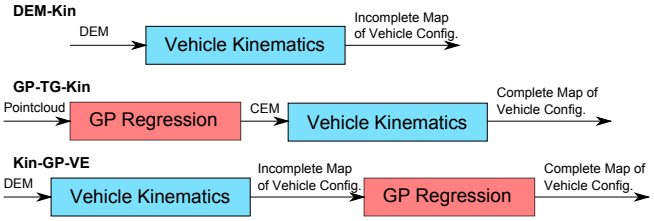

Fig. 2. Comparison of techniques to predict vehicle configuration.

We argue that better estimates can be obtained by directly estimating traversability over terrain data by learning vehicle response by experience, and this will be demonstrated experimentally in this paper. As such, we propose to perform GP regression over Vehicle Experience (Kin-GP-VE in Fig. 2) to obtain complete and continuous traversability maps.

Most recent work considered estimating traversability purely from vehicle experience [13]. The authors explored the possibility of building large scale traversability maps for a vehicle performing a repeated activity in a bounded environment. While the work demonstrated the ability to estimate traversability metrics using proprioceptive data in a GP framework, "blind" predictions were made in large areas with no data because no exteroceptive data were used in the traversability estimate, even arguably relevant data such as geometry of the terrain. This can result in large inaccuracies in the presence of large unexpected obstacles. For example, trees in the environment are not seen as obstacles.

The method proposed in this paper makes use of perceived terrain geometry through kinematic modeling of the rover chassis on DEMs built by on-board sensors. The combination of exteroceptive data with proprioceptive learning provides more complete and more accurate traversability maps.

III. Approach

In this paper, the prediction of vehicle attitude and chassis configuration angles is achieved using GP regression. In addition, as an alternative to state-of-the-art approaches utilizing comprehensive terrain and kinematic models, we employ a relatively simple implementation of both and instead focus on the explicit correlation in vehicle attitude and configuration during operation. By exploiting such correlations, we can make an estimate with lower Root Mean Squared Error (RMSE) of the vehicle attitude and configuration over an area given incomplete observations of such states.

As each choice of kernel function directly affects the nature of estimation in a GP framework [14], we propose to learn a kernel function to improve the accuracy in estimation over existing kernel functions. To better facilitate the direct estimation of traversability, we develop an architecture for estimating the kernel function based on vehicle experience in a manner that better represent the evolution of vehicle states and propagation of uncertainty. We perform experiments in an area that is representative of the type of terrain the rover is likely to encounter during operation, and record vehicle attitude and configuration over predefined areas. We learn

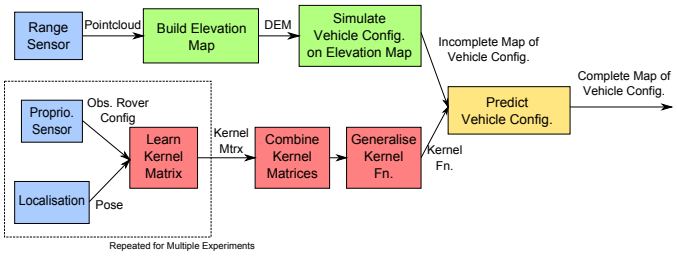

Fig. 3. System Architecture of Kin-GP-VE. Red modules indicate offline components for learning the kernel function. Green blocks indicate online vehicle configuration estimation using kinematics and corresponds to the blue block in Kin-GP-VE in Fig. 2. Yellow blocks indicate GP regression components for predicting vehicle configuration and corresponds to the red block in Kin-GP-VE in Fig. 2

separate kernel matrices for each vehicle response that we would like to predict in operation. As the vehicle is likely to traverse over different types of terrain, we combine the kernel matrices in a manner that maximizes entropy (or information) of the matrix. Furthermore, we generalize the combined kernel matrix into a GP framework for traversability estimation. In operation, we build a DEM by which we calculate the vehicle attitude and configuration on observable areas. We then perform a GP regression to determine a continuous representation of vehicle attitude and configuration over the entire area. An overview of our approach can be described as follows (see Fig. 3). First, the training phase consists in the following steps:

1) gathering vehicle attitude data (roll, pitch, yaw) with corresponding localization over several practice runs,
2) learning the kernel matrix based on vehicle attitude using Regularized Expectation Maximization (REM),
3) collaborating/combining kernel matrices from different experiments using Maximum Entropy Covariance Selection (MECS),
4) generalizing the kernel to other contexts using an auxiliary kernel function in a GP framework.

Once this training has been achieved, traversability estimation can be achieved on the rover by following these steps:

1) building a DEM from the point clouds acquired using a 3D sensor, e.g. RGB-D camera or stereovision,
2) estimating vehicle attitude on the DEM via a kinematics model, wherever the map is complete,
3) by using the covariance function learnt from experiments, predicting the vehicle attitude over the entire DEM using GPs.

A. Regularized Expectation Maximization (REM)

If a complete set of terrain data was available, the sample covariance matrix would represent a consistent and unbiased estimator of the covariance matrix of the data in the region encompassed by the dataset. But if only an incomplete set is available, various problems can arise from the estimation of the covariance matrix, such as non-guaranteed semi-definitiveness. In order to facilitate the estimation of covariance matrices from available data, an iterative method based on the Expectation Maximization (EM) algorithm [15] was developed to perform both the estimation of covariance matrices and the imputation of missing values.

In the EM algorithm, the parameters of the probability distribution are estimated from the incomplete dataset by maximizing the likelihood of the available data iteratively. The regular EM algorithm is typically described in 2 steps:

1) Expectation step - determining the expected value Q and covariance matrix $\tilde{K}$ of log-likelihood of the complete dataset based on the incomplete dataset and the parameter $\theta^{(\kappa)}$ which needs to be maximised:

$$\begin{aligned} &L = p(X, Z|\theta), \\ &Q\left(\theta|\theta^{(\kappa)}\right) = E\left(\log L|X, \theta^{(\kappa)}\right), \\ &\tilde{K}\left(\theta|\theta^{(\kappa)}\right) = \\ &\quad E\left[\left(\log L - Q\left(\theta|\theta^{(\kappa)}\right)\right)\left(\log L - Q\left(\theta|\theta^{(\kappa)}\right)\right)^T\right] \end{aligned} \tag{1}$$

where L is the likelihood function, X is the set of discrete observed values, Z are the missing discrete values, θ is the set of parameters describing the conditional distribution of Z given X.

2) Maximization step - The parameter θ of probability distribution is estimated from incomplete data by maximising the likelihood of the available data:

$$\theta^{(\kappa+1)} = \arg\max_{\theta} Q\left(\theta|\theta^{(\kappa)}\right)$$

Regularized EM consists of the same steps as the EM algorithm, but in each iteration and for each record of missing values, the inverse matrix in the conditional maximum likelihood estimate is replaced with a regularized inverse.

1) The conditional maximum likelihood estimation of the regression coefficients can be expressed as:

$$B = \tilde{K}_{aa}^{-1}\tilde{K}_{am} \tag{2}$$

where $\tilde{K}_{aa}$ and $\tilde{K}_{am}$ are the sub-matrices of the estimated covariance matrix $\tilde{K}\left(\theta|\theta^{(\kappa)}\right)$, which respectively consist of the estimated variances and covariances of variables from which data was observed, and cross-covariance of the variables that are missing.
2) The inverse matrix in the conditional maximum likelihood estimate was replaced with a regularized inverse:

$$\tilde{K}_{aa}^{-1} \leftarrow \left(\tilde{K}_{aa} + h^2 D\right)^{-1} \tag{3}$$

where $D = Diag\left(\tilde{K}_{aa}\right)$, and h is a scalar regularization parameter.

B. Maximum Entropy Covariance Selection (MECS)

In real-world applications the true kernel matrix is rarely known, and thus estimates must be determined based on correlations in a training set. Over numerous learning scenarios undertaken by the rover, kernel matrices of various

classes are accumulated. As the amount of proprioceptive data acquired from each experiment is relatively sparse and limited, it is desirable to combine all the information into a single estimator for each vehicle state in order to avoid poorly estimated or singular kernel matrices. Furthermore, we favored the use of methods based on the maximum entropy (ME) principle, which draws the inferences from the probability distribution that has the maximum entropy from the information that we do have [16].

We employ an adaptation of the MECS method [17] to combine the kernel matrices within each vehicle state in the available data. It combines kernel matrices by maximizing entropy in a multivariate distribution, thus accounting for the maximum uncertainty. This method considers the convex combinations of sample group kernel matrices, and selects the maximum variances of the kernel matrices given by an orthonormal projection basis that diagonalizes an unbiased linear mixture of the corresponding matrices. As the convex combination is always a linear operation over real numbers, the kernel matrix needs to be updated recursively as more learning data becomes available.

The algorithm for MECS for covariance combination is outlined as follows [17]:

1) find eigenvectors Φ_i of the summation of the covariance matrices $\tilde{K}_i$ and $\tilde{K}_j$.
2) calculate variance contribution from $\tilde{K}_i$ and $\tilde{K}_j$ on the Φ_i basis:

$$\begin{aligned} \mathrm{diag}(Z^i) &= \mathrm{diag}\left[(\Phi_i)^T \tilde{K}_i \Phi_i\right] = \left[\zeta_1^i, \zeta_2^i, ..., \zeta_j^i\right] \\ \mathrm{diag}(Z^j) &= \mathrm{diag}\left[(\Phi_i)^T \tilde{K}_j \Phi_i\right] = \left[\zeta_1^j, \zeta_2^j, ..., \zeta_j^j\right], \end{aligned} \tag{4}$$

3) form new variance matrix to maximise entropy:

$$Z_i = \mathrm{diag}\left[\max\left(\zeta_1^i, \zeta_1^j\right), ..., \max\left(\zeta_j^i, \zeta_j^j\right)\right], \tag{5}$$

4) determine combined covariance matrix:

$$K_i = \Phi_i Z_i \left(\Phi_i\right)^T. \tag{6}$$

C. Gaussian Processes

1) GP Framework for Traversability Estimation: To estimate missing data we use Gaussian Processes (GP) to learn the underlying model of spatially correlated data with uncertainty [14]. Gaussian approaches are defined as a normally distributed probability density function characterized by a mean $m(X)$ and covariance function $k(X, X')$

$$\begin{aligned} m(X) &= E[f(X)] \\ k(X, X') &= E[(f(X) - m(X))(f(X') - m(X'))] \end{aligned} \tag{7}$$

where $X = \begin{bmatrix} x \\ y \end{bmatrix}$, denoting our input variable of x and y coordinates in the Cartesian space.

We set up the traversability estimation scenario as a GP regression problem. Since the joint distribution of any finite number of random variations of a GP is Gaussian, the joint distribution of the training data z and test data $f*$ can be given as:

$$\begin{bmatrix} z \\ f* \end{bmatrix} \sim N\left(0, \begin{bmatrix} K(X,X) + \sigma_n^2 I & K(X, X_*) \\ K(X, X_*) & K(X_*, X_*) \end{bmatrix}\right) \tag{8}$$

The posterior and covariance can be given respectively as

$$\bar{f}_* = K(X_*, X)[K(X,X) + \sigma_n^2 I]^{-1} z \tag{9}$$

$$\begin{aligned} &cov(f_*) \\ &= K(X_*, X_*) - K(X_*, X)[K(X,X) + \sigma_n^2 I]^{-1} K(X, X_*) \end{aligned} \tag{10}$$

For n training points and n_* test points, $K(X, X_*)$ represents the $n \times n_*$ covariance matrix evaluated at all the pairs of training and test points. Thus, for each vehicle state (pitch=ϕ, roll=θ and chassis configuration angles α_i) we can formulate separate GP estimators for each output by setting the input variable as the vehicle position and training data as $z = [\phi, \theta, \alpha_i]$. To predict z over different yaw angles, we discretize the training inputs and outputs into 8 yaw angle directions to limit the amount of training data required. GP regression is then performed over the training and test data to predict z, and compared with the data obtained from experiments.

2) Generalizing Kernel Matrix in GP framework: To incorporate the learnt covariance matrix for use in the GP prediction framework, we generalize the covariance matrix into a functional form with the use of an auxiliary kernel function $k(.,.)$ that takes a set of X as inputs. Our strategy is to use a method similar to the Nyström method for approximating eigenfunctions [18]:

$$k(X, X') = \sum_{i=1}^{N} \lambda_i \phi_i(X) \phi_i(X') \tag{11}$$

where $N \leq \infty$, $\lambda_1 \geq \lambda_2 \geq ... \geq 0$ are the eigenvalues, and ϕ_i are the eigenfunctions with the operator whose kernel is k.

$$\int k(X', X) \phi_i(X) p(X) dX = \lambda_i \phi_i(X') \tag{12}$$

where $p(X)$ is the probability density of the input vector X. To approximate the eigenfunction equation over an independent and identically distributed sample of the input vector X from $p(X)$, we can substitute the integral in Eq. (12) with an empirical average. This leads to the matrix eigenproblem, to which we generalize the covariance matrix in the GP framework using:

$$KU = U\Lambda \tag{13}$$

where K is the covariance matrix, U is the column of orthonormal eigenvectors, and Λ is the diagonal matrix of eigenvalues $\lambda_1 \geq \lambda_2 \geq ... \geq 0$. Performing an eigendecomposition on K gives:

$$K = U\Lambda U^T \tag{14}$$

Consequently, the scaled eigenvectors V are obtained as:

$$V = U\Lambda^{1/2}. \tag{15}$$

We can approximate the i^{th} eigenvector using Gaussian Processes with the auxiliary kernel $k(.,.)$, and express as a scaled eigenfunction

$$\phi_i(X) = \sum_{j=1}^{N} k(X, X_j) b_{i,j}, \tag{16}$$

where $b_{i,j}$ are the weights and can be expressed as $(b_{i,1}, ..., b_{i,N})^T = (K + \gamma I)^{-1} v_i$. The jitter term γI is introduced to stabilize the inverse term. Using the approximated scaled eigenfunctions, the kernel function is generalized as:

$$\begin{aligned} l(X, X') &= \sum_i \phi_i(X)\phi_i(X')) \\ &= k(X, X_j) (K + \gamma I)^{-1} K (K + \gamma I)^{-1} k(X', X_j) \end{aligned} \tag{17}$$

The learnt kernel function can then be implemented in a GP framework for regression to predict vehicle states.

IV. Implementation

A. Platform - Mawson Rover

Mawson is a 6-wheeled rover with a rocker-bogie chassis and individual steering motors on each wheel (Fig. 4). Onboard sensors include:

- 2 color cameras and a RGB-D camera (Microsoft Kinect^{TM}) mounted on a pan-tilt unit, tilted down about $18°$, which is used primarily for terrain modeling.
- 2 Hall-effect encoders and a potentiometer on the rear bogie mechanisms and rocker differential, respectively, to measure the configuration of the chassis.
- A 6-DOF Inertial Measurement Unit (IMU) used to measure roll, pitch, and yaw of the rover.

In our experiments, localization was performed using the Intersense IS-1200 motion capture system, which uses a combination of camera and IMU data to determine the 6-DOF sensor pose $(x, y, z, \phi, \theta, \psi)$ (where ϕ is the roll, θ the pitch and ψ the yaw) with respect to a constellation of fiducials in the environment[1]. This system provides 2 cm-accuracy localization.

[1]note the experiments were conducted indoors, on unstructured terrain.

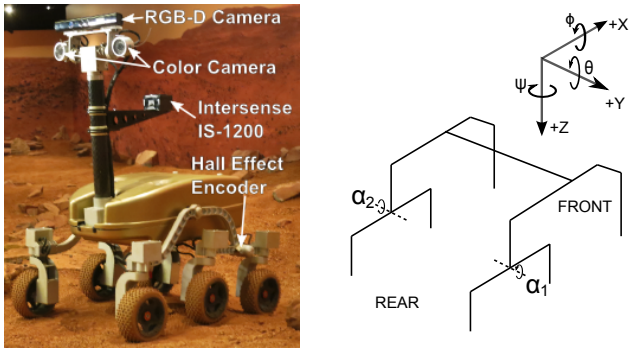

(a) (b)

Fig. 4. (a) Mawson Rover. (b) Chassis Configuration.

Point-clouds provided by the RGB-D camera are used to build the elevation maps. Although this sensor may not be appropriate for some outdoor operations, the point-cloud can also be obtained from other sensors such as stereovision without affecting the conclusion of this study.

In order to associate the point clouds acquired by the RGB-D camera with the Intersense localization, we performed exteroceptive calibration between the two sensors to estimate the transformation between them. We used the technique described in [19].

B. Kinematics Model

To predict vehicle attitude angles and chassis configuration of the rover given a (2D) position and orientation (yaw angle) on an existing elevation map, we used a method adapted from [6], which assumes the terrain to be rigid. Although this relatively simple kinematic model does not take into account the dynamics of the platform, it is sufficient in this approach since the rover operates at low speeds ($\approx 0.05 - 0.15m/s$). In addition, Kin-GP-VE allows for more complex kinematic/dynamic models to be integrated with minor changes in the formulation.

To determine wheel elevation (z_i) given rover position (x, y, z), orientation (ϕ, θ, ψ) and configuration (q), a function was defined using kinematic constraints. In this implementation, the wheel contact point with the ground was assumed to be the surface normal of the ground to the cylindrical wheel [20]:

$$z_i = f(x, y, z, \phi, \theta, \psi, q) \tag{18}$$

An error function (η) was defined as the difference (E_i) between the wheel elevation (z_i) and the projected contact point of the wheel and the ground on the elevation map $(z_{terrain})$, and the objective function calculated by taking the norm of the error vector:

$$E_i = z_i - z_{terrain} \tag{19}$$

$$\eta(z, \phi, \theta, q) = E^T E \tag{20}$$

Finally, the nonlinear optimization problem to find the free parameters (z, ϕ, θ, q) was solved via a Golden Section search and parabolic interpolation [21].

C. Test Environment

The experiments were conducted at the Marsyard, a Mars analogue terrain hosted inside the Powerhouse Museum in Sydney, Australia. The Marsyard is approximately $15m \times 8m$ and contains various types of rocks, gravel, as well as varying degrees of slope. The typical obstacle size in the Marsyard is approximately 0.05 to $0.2m$ in radius, which presents a considerable challenge in traversability as the wheel radius of the rover is $0.05m$. Three areas within the Marsyard were selected for experiments, which are illustrated in Fig. 5 by the shaded areas.

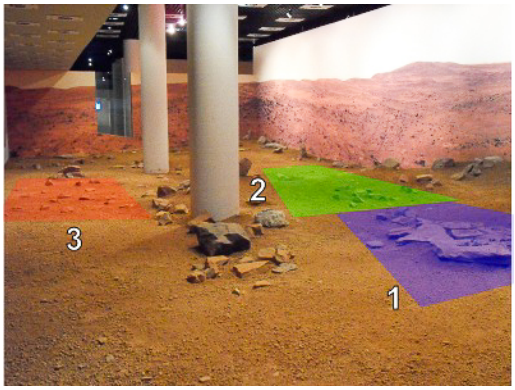

Fig. 5. Marked terrain areas on Marsyard for kernel learning. Area 1 is highlighted in blue as the $3m \times 3m$ rough terrain area on the right (blue). Area 2 is highlighted in green as the $3m \times 3m$ slope area on the right, and Area 3 is highlighted in red as the $2.5m \times 2.5m$ rocky area on the left (red).

D. Training for Kernel Learning

Training for kernel learning consisted of executing terrain traversals in a grid pattern to cover each of the three areas of the Marsyard, as defined in Fig. 5, while recording vehicle configurations using the Intersense IS-1200 and hall effect encoders. Fig. 6 shows an example of the rover trajectory when covering Area 1 for this training stage. From these data, we imputed the measurements at missing locations while estimating the covariance matrix using REM, and repeated the procedure for each output variable. To generalise the learnt kernel matrix into a functional form, an additive kernel composed from Sq-Exp and NN kernels was used as the auxiliary function to initialise the process.

E. GP Regression Training Inputs and Outputs

We used a separate GP for each variable in the training output. In each of the GP estimators, the training input is defined as the vehicle position X and the training output z is defined as the vehicle roll (ϕ), pitch (θ) or rear bogie angles $(\alpha_{1,2})$ as defined in Fig. 4(b):

$$X = \begin{bmatrix} x \\ y \end{bmatrix}, z = \{\phi, \theta, \alpha_1, \alpha_2\} \tag{21}$$

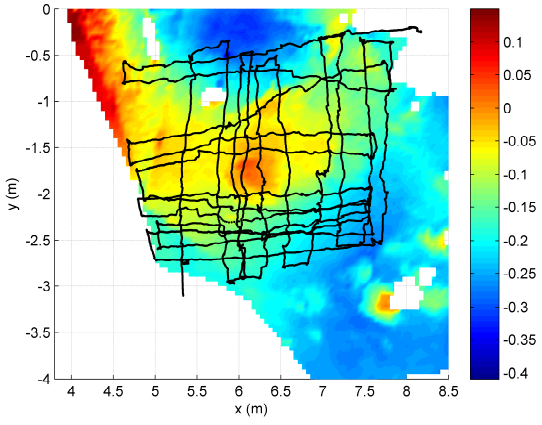

Fig. 6. Vehicle trajectory on geo-referenced elevation map in Area 1.

V. Experiments and Results

To validate experimentally the proposed approach, we evaluated the accuracy of the predictions achieved by our method and by state-of-the-art techniques discussed in Sec. II. These predictions were compared with the measurements of attitude and configuration angles obtained with the rover's localization system and hall effect encoders, taken as ground truth. This evaluation was made with approximately 12000 points of ground truth data on each testing area, over a grid resolution of $5cm$, which is approximately equivalent to the radius of the rover's wheel. We then computed the Root-Mean-Squared Error (RMSE) obtained for each angle and each area. 2 stages of validation were performed.

A. Validation Part 1: Learnt Kernel

To validate the performance of the learnt kernel function against state-of-the-art kernel functions on the most basic level, we trained the hyperparameters of the Squared Exponential (Sq. Exp.) and Neural Network (N.N.) kernel functions over the same 70% of the recorded vehicle states from traversals in each area in the Marsyard that were used for our learnt kernel function. The trained GP was then used to predict the vehicle's attitude and configuration angles over the entire grid area and cross-validated with the remaining 30% of data.

Table I shows a comparison of the RMSE in the prediction of each vehicle configuration angle (w.r.t. the ground truth) using the different kernel functions, for the three areas labeled in Fig. 5. The last two rows of the table summarize the improvement obtained using our learnt kernel, compared to Sq. Exp. and N.N. (in %). We observe that the error is significantly reduced using the learnt kernel function compared with the Sq. Exp. or N.N. kernel functions. In particular, the RMSE in vehicle pitch estimation improved by 17% and 34% using the learnt kernel function over the Sq. Exp. and N.N. kernel functions respectively. The table also shows consistent improvement in estimation of other vehicle configuration angles over the two state-of-the-art kernel functions.

TABLE I

Prediction Errors (in deg.) Based on Vehicle Experience

Area	Kernel Used	RMSE Roll	RMSE Pitch	RMSE L. Bogie	RMSE R. Bogie
1	Learnt	3.87	4.62	5.93	5.72
	Sq. Exp. Iso.	4.23	4.98	6.51	5.78
	N.N.	5.60	5.27	6.86	5.82
2	Learnt	1.32	1.73	5.37	4.17
	Sq. Exp. Iso.	1.75	2.78	6.33	5.09
	N.N.	2.66	6.64	6.84	5.64
3	Learnt	1.34	1.93	3.83	4.49
	Sq. Exp. Iso.	1.41	2.08	4.18	4.70
	N.N.	1.5491	2.34	4.27	4.68
	% Imprv. Sq.Exp.	12.67	17.47	10.89	7.81
	% Imprv. N.N.	31.47	34.70	15.15	10.63

TABLE II

PREDICTION ERRORS (IN DEG.) BASED ON VEHICLE KINEMATICS AND GP ESTIMATION (KIN-GP-VE)

Area	Kernel Used	RMSE Roll	RMSE Pitch	RMSE L. Bogie	RMSE R. Bogie
1	Learnt	4.18	5.02	5.18	6.02
	Sq. Exp. Iso.	5.95	6.50	5.34	5.99
	N.N.	5.03	6.10	5.40	6.22
2	Learnt	3.02	3.02	5.90	5.83
	Sq. Exp. Iso.	3.01	2.78	6.66	6.01
	N.N.	3.01	2.78	6.87	6.52
3	Learnt	1.71	2.84	5.45	5.24
	Sq. Exp. Iso.	1.93	2.65	6.42	6.42
	N.N.	1.75	2.45	6.32	6.23
% Imprv. over Sq. Exp.		13.61	2.45	9.79	6.94
% Imprv. over N.N.		6.22	-2.16	10.67	9.84

B. Validation Part 2: Kin-GP-VE

We also evaluated the ability of our approach to predict vehicle configuration over the vehicle state space using exteroceptive sensing. We first performed kinematic modeling (as described in Sec. IV-B) over an elevation map built using a Kinect snapshot of the terrain. This data was then used to train the hyperparameters of the GP, which was then used to predict vehicle configuration over the entire area (see Kin-GP-VE process described in Figs. 2 & 3). This prediction via GP regression was achieved using each of the three kernel functions and cross-validated with proprioceptive data obtained during traversals.

The corresponding RMS errors are summarized in Table II. It shows a clear improvement in estimates using the learnt kernel function compared to the Sq. Exp. and N.N. kernel functions, with improvements in RMSE up to 14% and 11% respectively. Note that the RMSE in vehicle attitude and configuration is higher in Area 2 than in Area 3. This can be attributed to larger areas of occlusion from larger obstacles in Area 2, as well as more loose terrain leading to wheel sinkage, which is not accounted for in the kinematic model.

Fig. 7 shows a cross-section view of the vehicle pitch predicted using Kin-GP-VE and DEM-Kin over Area 2. It can be seen from $x = 10.9m$ to $11.2m$ that the roll angle estimated using DEM-Kin significantly deviates from the ground truth. This may be attributed to terrain deformation experienced during vehicle traversal, which is not considered in the kinematic model since it assumes the terrain to be rigid (see to Section IV-B). The prediction made using the learnt kernel function is found to be closer to the ground truth than Sq. Exp. and N.N. in the majority of cases, with the exception of RMSE in pitch, in which the N.N. kernel function performs slightly better in Areas 2 and 3.

C. Comparison with GP-TG-Kin

Table III shows the performance of kinematics modeling applied on terrain models estimated via GP regression (GP-TG-Kin, see Fig. 2). The last row of the table shows the improvement over GP-TG-Kin obtained using our approach (Kin-GP-VE). We can see that the RMSE in vehicle configuration estimates using the Sq. Exp. and N.N. kernel functions

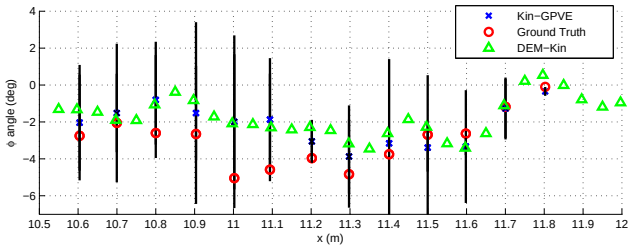

Fig. 7. Roll estimated by GP (Kin-GP-VE, blue cross), and by kinematics over DEM (DEM-Kin, green triangle), against ground truth (red circle). Black error bars denote the uncertainty in the GP prediction. Cross section was taken at $y = -1.3$ to $-1.2m$ in the black boxed area in Fig. 9.

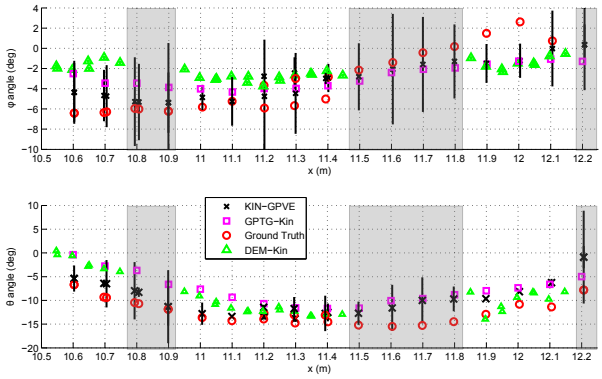

Fig. 8. Roll (top) and pitch (bottom) predicted using our approach Kin-GP-VE (black cross), using kinematic modeling over a GP-predicted terrain (GP-TG-Kin, pink square), and using kinematic modelling on raw elevation map (DEM-Kin, green dot), against ground truth (red circle). The grey shaded areas denote occluded areas. Cross section was taken at $y = -0.4$ to $-0.3m$ in the black boxed area in Fig. 9.

are lower in GP-TG-Kin than in Kin-GP-VE. GP-TG-Kin estimates terrain geometry data with occlusions, whereas Kin-GP-VE estimates vehicle configuration, which has more missing data. As the transformation from terrain geometry to vehicle configuration is dependent on the contact between all six wheels and the terrain, there is more missing data in the vehicle configuration space because of all situations where the contact with at least one wheel corresponds to an occluded area of the terrain. This contributes to better performance of GP-TG-Kin over Kin-GP-VE using the standard kernel functions. However, it can be seen that the estimation made using the *learnt* kernel function in the Kin-GP-VE framework still shows an improvement over both kernel functions in the GP-TG-Kin framework consistently over all vehicle configuration angles.

Fig. 8 and Table IV specifically compare the relative performance of the different methods in occluded sections vs. non-occluded sections of Area 2. It can be seen that in the occluded region from $x = 10.75$ to $10.95m$, and from $x = 11.45$ to $11.85m$ the prediction made using Kin-GP-VE is closer to ground truth than using GP-TG-Kin.

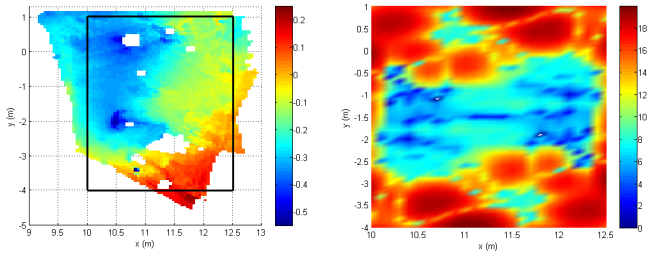

(a) (b)

Fig. 9. (a) Elevation map of Area 2 with black box indicating area of estimation. (b) Uncertainty in roll estimate.

TABLE III

PREDICTION ERRORS (IN DEG.) BASED ON GP TERRAIN MODELING AND VEHICLE KINEMATICS (GP-TG-KIN)

Area	Kernel Used	RMSE Roll	RMSE Pitch	RMSE L. Bogie	RMSE R. Bogie
1	Sq. Exp. Iso.	5.45	6.87	6.64	7.82
	N.N.	5.68	6.83	6.25	6.91
2	Sq. Exp. Iso.	4.90	4.42	6.28	7.58
	N.N.	3.72	4.13	5.75	7.89
3	Sq. Exp. Iso.	2.81	3.83	5.15	5.46
	N.N.	2.80	3.82	5.33	5.73
% Imprv. using Kin-GP-VE		30.68	27.19	5.66	16.18

VI. CONCLUSION

This paper introduced a novel method for predicting the attitude and configuration angles of a planetary rover over rough terrain, thereby estimating terrain traversability. The proposed method estimates the vehicle configuration in a GP framework by learning a kernel function from vehicle experience. The experimental validation of the method showed marked improvement over state-of-the-art techniques, both in its ability to provide estimates in occluded areas and in its accuracy overall. In particular, the validation process consistently showed increased accuracy with our learnt kernel function compared to using standard kernel functions.

All methods compared in the experiments of this paper rely on the same state-of-the-art kinematics model, therefore, they are affected in the same way by its limitations. This is exemplified in the top graph of Fig. 9, between $x = 11.8m$ and $x = 12.1m$ where the GP prediction error is consistent with the kinematic model error, which is likely due to the assumption that the terrain is rigid. However, this assumption is violated in low cohesion soil or over unstable rocks. Therefore, further improvement in the accuracy of prediction of vehicle configuration would require a kinematic and dynamic model that account for non-rigid terrains. This will be considered in future work.

TABLE IV

ATTITUDE PREDICTION ERRORS (IN DEG.) OF KIN-GP-VE IN OCCLUDED VS. OBSERVABLE AREAS

Area	Kernel Used	Occluded		Non-Occluded	
		RMSE Roll	RMSE Pitch	RMSE Roll	RMSE Pitch
1	Learnt	6.78	7.65	4.01	4.78
	Sq. Exp. Iso.	7.67	7.85	5.52	6.01
	N.N.	7.70	8.03	4.82	5.70
2	Learnt	7.32	8.25	2.84	2.78
	Sq. Exp. Iso.	8.12	8.98	2.78	2.60
	N.N.	8.43	8.73	2.88	2.64
3	Learnt	3.08	3.52	1.52	2.34
	Sq. Exp. Iso.	3.47	3.89	1.78	2.18
	N.N.	3.20	3.47	1.53	2.10
% Imprv. over Sq. Exp.		10.90	6.73	13.27	2.07
% Imprv. over N.N.		9.62	2.93	6.28	-0.20

REFERENCES

[1] S. Singh, K. Schwehr, R. Simmons, T. Smith, A. Stentz, V. Verma, and A. Yahja, "Recent progress in local and global traversability for planetary rovers," in *Proc. IEEE ICRA*, 2000.

[2] S. B. Goldberg, M. W. Maimone, and L. Matthies, "Stereo vision and rover navigation software for planetary exploration," in *Proc. IEEE Aerospace Conf.*, 2002.

[3] V. Molino, R. Madhavan, E. Messina, A. Downs, S. Balakirsky, and A. Jacoff, "Traversability metrics for rough terrain applied to repeatable test methods," in *Proc. IEEE/RSJ IROS*, 2007.

[4] G. Ishigami, K. Nagatani, and K. Yoshida, "Path planning and evaluation for planetary rovers based on dynamic mobility index," in *Proc. IEEE/RSJ IROS*, 2011.

[5] S. Lacroix, A. Mallet, D. Bonnafous, G. Bauzil, S. Fleury, M. Herrb, and R. Chatila, "Autonomous rover navigation on unknown terrains: Functions and integration," *Int. J. Robotics Research*, vol. 21, no. 10-11, pp. 917–942, 2002.

[6] M. Tarokh and G. McDermott, "Kinematics modeling and analyses of articulated rovers," *IEEE Trans. Robotics*, vol. 21, no. 4, pp. 539–553, 2005.

[7] C. A. Brooks and K. Iagnemma, "Self-supervised terrain classification for planetary surface exploration rovers," *J. of Field Robotics, Special Issue on Space Robotics, Part I*, vol. 29, no. 3, pp. 445–468, 2012.

[8] D. Helmick, A. Angelova, and L. Matthies, "Terrain adaptive navigation for planetary rovers," *J. Field Robotics*, vol. 26, no. 4, pp. 391–410, 2009.

[9] A. Kelly and A. Stentz, "Analysis of requirements for high speed rough terrain autonomous mobility part 1: Throughput and response," in *Proc. IEEE ICRA*, 1997.

[10] R. Hadsell, J. A. Bagnell, D. Huber, and M. Hebert, "Accurate rough terrain estimation with space-carving kernels," in *Robotics: Science and Systems*, 2009.

[11] S. Vasudevan, F. Ramos, E. Nettleton, and H. Durrant-Whyte, "Large-scale terrain modeling from multiple sensors with dependent gaussian processes," in *Proc. IEEE/RSJ IROS*, 2010.

[12] K. Ho, T. Peynot, and S. Sukkarieh, "Analysis of terrain geometry representations for traversability of a mars rover," in *NCSS/NSSA Australian Space Science Conference*, 2011.

[13] S. Martin, L. Murphy, and P. Corke, "Building large scale traversability maps using vehicle experience," in *Proc. Int. Symp. Experimental Robotics*, 2012.

[14] C. E. Rasmussen and C. K. I. Williams, *Gaussian Processes for Machine Learning*. Cambridge, MA: The MIT Press, 2006.

[15] A. P. Dempster, N. M. Laird, and D. B. Rubin, "Maximum likelihood from incomplete data via the em algorithm," *J. Royal Statistical Society. Series B (Methodological)*, vol. 39, no. 1, pp. 1–38, 1977.

[16] E. T. Jaynes, "On the rationale of maximum-entropy methods," in *Proc. IEEE*, vol. 70, 1982, pp. 939–952.

[17] C. Thomaz, D. Gillies, and R. Feitosa, "A new covariance estimate for bayesian classifiers in biometric recognition," *IEEE Trans. Circuits and Systems for Video Technology*, vol. 14, no. 2, pp. 214–223, 2004.

[18] C. K. I. Williams and M. Seeger, "Using the nystrom method to speed up kernel machines," *Advances in Neural Information Processing Systems*, 2001.

[19] J. P. Underwood, A. Hill, T. Peynot, and S. J. Scheding, "Error modeling and calibration of exteroceptive sensors for accurate mapping applications," *J. Field Robotics*, vol. 27, no. 1, pp. 2–20, 2010.

[20] K. Iagnemma and S. Dubowsky, "Vehicle wheel-ground contact angle estimation: with application to mobile robot traction control," in *Proc. Int. Symp. Advances in Robot Kinematics*, 2000.

[21] R. P. Brent, *Algorithms for Minimization without Derivatives*. Englewood Cliffs, N.J.: Prentice-Hall, 1973.